

Principles of Parametric Temporal Imaging—Part II: System Performance

Corey V. Bennett, *Student Member, IEEE* and Brian H. Kolner, *Member, IEEE*

Abstract—The waveform manipulation technique known as temporal imaging can expand or compress signals in time while maintaining the shape of their envelope profiles. The temporal imaging system is analogous to that of its spatial counterpart, with dispersive propagation performing the role of diffraction and quadratic phase modulation in time acting as a “time lens.” Recent work has concentrated on time lenses produced by the parametric mixing of the dispersed input signal with a linearly chirped optical pump pulse because of the broad bandwidth, and thus fine temporal resolution, that can be obtained. In a previous paper, we presented the numerous parametric imaging configurations that are possible and drew temporal ray diagrams to illustrate their operation. In this paper, we study the performance of these systems. Resolution, field of view, number of resolvable features, and distortions particular to this approach are discussed.

Index Terms—Dispersive propagation, frequency mixing, phase modulation, temporal imaging, time lens, ultrafast measurement, ultrafast pulse propagation.

I. INTRODUCTION

TEMPORAL IMAGING [1]–[7] is a technique that enables manipulation of a waveform’s time scale in a manner analogous to the spatial scaling performed in a conventional imaging system. Generation, manipulation, and measurement of arbitrarily shaped optical waveforms with ultrafast temporal detail is a challenging field of growing importance. These tasks are especially challenging for long single-transient waveforms with ultrafast temporal detail, or equivalently signals with a large time-bandwidth product. Imaging the waveform in time can produce a magnified or demagnified version with the same envelope profile, thus improving the performance of the waveform generation or recording system. This process is fundamentally single-shot, producing a scaled replica of the entire input field of view for each occurrence of the time lens. It is therefore expected that this technology will lead to a new class of ultrafast transient recorders and a new technique for producing shaped ultrafast waveforms. Numerous temporal imaging configurations possible with a parametric time lens were presented in a previous paper [8]. Temporal ray diagrams were used to illustrate

their operation. This paper will investigate the performance of these systems.

Temporal imaging is based on the analogy between spreading of a beam due to paraxial diffraction and spreading of a pulse due to narrowband dispersion. Diffraction causes a beam of light to spread in the transverse coordinates (x, y) as it propagates a distance z . Group velocity dispersion (GVD) $\beta'' = d^2\beta(\omega)/d\omega^2|_{\omega=\omega_0}$ causes a pulse of light to spread in the local time coordinate $\tau = t - t_0 - (z - z_0)/v_g(\omega_0)$ as it propagates with group velocity $v_g(\omega_0)$ a distance $\xi = z - z_0$ (or, equivalently, through a total group delay dispersion (GDD) $\phi'' = \xi\beta''$). The equations describing these two phenomena are the same form [9]–[13], and each can be shown to impart a quadratic phase in its respective frequency domain [6]. Dispersion can therefore perform a similar role in temporal imaging systems as does paraxial diffraction in spatial systems.

A lens in space imparts a quadratic spatial phase to a wavefront [14], thus any process that imparts a quadratic temporal phase (i.e., a linear frequency chirp $d\omega/d\tau$) can be used as a time lens. We may characterize the strength of the phase modulation with a focal GDD, $\phi_f'' \equiv -(d\omega/d\tau)^{-1}$, which is the dispersion required to remove the imparted phase profile. A figure of merit for the resolution of a system utilizing this lens is the temporal f -number, $f^\# = \omega_0/\Delta\omega$, where ω_0 is the carrier frequency out of the time lens and $\Delta\omega$ is the bandwidth it imparts [6], [15]. The first optical time lenses were produced using electrooptic phase modulators [16]–[23], but technical challenges in producing the required bandwidth limited the usefulness of these systems. Much broader bandwidth is available from ultrafast optical sources. This has provided motivation for the study of time lenses produced by mixing the input signal with a chirped optical pump pulse in a nonlinear crystal [8], [24]–[26]. Assuming ideal phase matching over the entire bandwidth, the frequency-shifted output is proportional to the product of the time lens input signal and the chirped pump pulse. The imparted phase profile of the pump produces the necessary time lens action and the amplitude profile of the pump acts as a shutter by limiting the duration of the transmitted signal.

A spatial imaging system [Fig. 1(a)] is constructed by cascading diffraction, a lens, and further diffraction in the proper balance to satisfy the familiar imaging condition $1/d_1 + 1/d_2 = 1/f$. This assumes that the index of refraction on each side of the lens has the same constant value, as is often the case, and thus the rate of diffraction is the same. The output envelope profile $E(x/M)$ is then a scaled replica of the input $E(x)$, where the magnification is given by the ratio of propagation distances $M = -d_2/d_1$. A temporal imaging system [Fig. 1(b)] is similarly constructed by cascading dispersion, a time lens, and further dispersion. When

Manuscript received December 29, 1999. This work was supported in part by the Department of Energy’s Lawrence Livermore National Laboratory under Contract W-7405-Eng-48, the LLNL Photonics Group under Laboratory Directed Research & Development Grant 98-ERD-027, the National Science Foundation, and the David and Lucile Packard Foundation.

C. V. Bennett is with the Electrical Engineering Department, University of California at Los Angeles, and the Electronics Engineering Division, Lawrence Livermore National Laboratory, Livermore, CA 94551 USA.

B. H. Kolner is with the Department of Applied Science, University of California at Davis, Davis, CA 95616 USA.

Publisher Item Identifier S 0018-9197(00)04442-0.

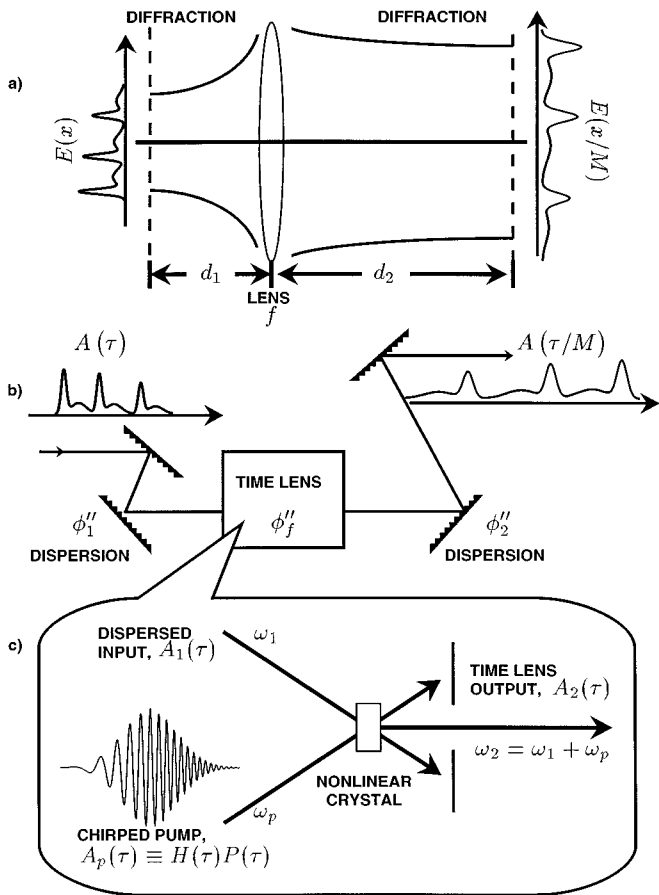


Fig. 1. (a) Spatial and (b) temporal imaging systems. This paper will concentrate on temporal systems using (c) a time lens constructed through the mixing of the dispersed input signal $A_1(\tau)$ with a chirped pump $A_p(\tau)$.

these processes are balanced in accordance with the temporal imaging condition

$$\frac{1}{\phi_1''} + \frac{1}{\phi_2''} = \frac{1}{\phi_f''} \quad (1)$$

an imaging system is formed with a magnification

$$M = -\frac{\phi_2''}{\phi_1''} \quad (2)$$

where ϕ_1'' and ϕ_2'' are the GDDs before and after the time lens, respectively.

Although it is unlikely to occur in a real physical system, it's interesting to note that, in the situation where the GVD β'' is constant, it factors out, producing an imaging condition and magnification that again depend solely on the distances involved. This is because both spatial and temporal imaging involve the balancing of the natural phase accumulated during propagation in space with an intentional phase-modulation process, be it a transverse spatial modulation or a modulation in time. Since GVD typically changes as the signal propagates through different components and is most likely not the same on each side of the lens, it is easier to measure propagation in terms of the total GDD through which the signal has propagated instead of physical propagation distances.

The time lens in Fig. 1(c) is produced by noncollinear sum-frequency mixing of a linearly chirped pump pulse

$A_p(\tau) \equiv H(\tau)P(\tau)$ (defined below) at a carrier frequency ω_p with the dispersed input signal $A_1(\tau)$ at ω_1 . To simplify the analysis, it is convenient to separate the pump envelope profile $A_p(\tau)$ into its phase function

$$H(\tau) = \exp\left(\frac{-i\tau^2}{2\phi_f''}\right) \quad (3)$$

and its amplitude profile (or pupil function) $P(\tau)$. In the case of ideal phase matching, the time lens output has an envelope proportional to the input and pump

$$A_2(\tau) \propto A_1(\tau)A_p(\tau) = A_1(\tau)H(\tau)P(\tau) \quad (4)$$

but at a new carrier frequency $\omega_2 = \omega_1 + \omega_p$. The pump's phase function $H(\tau)$ imparts the frequency chirp necessary to produce a time lens and the amplitude profile $P(\tau)$ limits the duration of the modulation process and thus also limits the bandwidth that is imparted. This produces a finite impulse response even for an ideal system. Temporal imaging systems can have other bandwidth limitations which will also modify the resolution and limit the field of view. For systems based on parametric conversion, a dominant filtering effect results from the parametric conversion process itself. How filtering effects restrict the performance of temporal imaging systems will be the main focus of this paper.

The frequency chirp of the pump pulse can also be imparted using other parametric processes. Numerous imaging system configurations possible with both sum- and difference-frequency generation (SFG and DFG) systems have been analyzed [8]. DFG systems introduce a complex conjugate to the analysis, changing the sign in the imaging condition of the required input dispersion for the "Pump-Input" configurations and the sign of the focal dispersion for the "Input-Pump" configurations. This changes how spectral components propagate through the imaging system, but SFG and DFG temporal imaging systems can still be configured to produce the same temporal image intensity profiles. In general, the temporal results of spectral filtering effects can change depending on the type of time lens and system configuration used. Depending on where the filtering occurs in the system, the effect in a DFG system may be time reversed from that of the SFG case. Assuming the filter function is symmetric about the carrier makes this distinction inconsequential. We will investigate SFG systems only, although the conclusions apply to the DFG systems as well.

II. IDEAL RESOLUTION

In a traveling-wave coordinate system, the response at time τ to an impulse at τ_0 of an ideal temporal imaging system with a finite pupil function (pump profile) $P(\tau)$ is $h(\tau; \tau_0) = C(\tau)\tilde{h}(\tau - M\tau_0)$, where

$$C(\tau) = \frac{1}{\sqrt{M}} \exp\left(\frac{-i\tau^2}{2M\phi_f''}\right) \quad (5)$$

$$\tilde{h}(\tau - \tau_0) = \frac{1}{2\pi\phi_2''} \int_{-\infty}^{+\infty} P(\tau') \exp\left[\frac{-i\tau'(\tau - \tau_0)}{\phi_2''}\right] d\tau' \quad (6)$$

and $\tau'_0 = M\tau_0$ is the magnified output time [6]. The first function, $C(\tau)$, scales the amplitude of the response to conserve energy and contains the imparted time lens frequency chirp, reduced by the magnification, which remains in the temporal image. The impulse response amplitude profile $\tilde{h}(\tau - \tau'_0)$ is given by the Fourier transform of the pump profile in a scaled and shifted coordinate system. For an arbitrary input signal, the output can be written as a superposition integral of the response $h(\tau; \tau_0)$ weighted by the input signal $A_{\text{in}}(\tau_0)$. The linear chirp term can be factored out and the expression simplifies to a convolution of the impulse response profile with the ideal magnified image

$$A_{\text{out}}(\tau) = C(\tau)[\tilde{h}(\tau) * A_{\text{in}}(\tau/M)]. \quad (7)$$

We will find in the next section that spectral filtering effects, common in ultrafast systems, can modify this result.

It should be noted that the system is approximated as time-invariant in order to express the output in the convolution form of (7). This simplifies the study of the system resolution but it does not accurately predict the roll-off in the image that limits the field of view (see Section IV).

A practical choice of resolution criteria depends on the application. One useful definition is to consider two pulses “resolved” when they are separated at the output by the width of the system’s impulse response. Consider a time lens pump that is initially a transform-limited Gaussian pulse with width $\Delta\tau_{p_0}$ and bandwidth $\Delta\omega_p$. The pump pulse can then be dispersed to obtain the required linear frequency chirp while simultaneously increasing the pulse duration. Large spreading of the pump pulse produced by propagating it through a GDD ϕ_p'' will create a time lens with a duration $\Delta\tau_p \approx |\phi_p''|\Delta\omega_p$ and a focal GDD $\phi_f'' \approx -\phi_p''$ [8]. For an ideal imaging system with large magnification $|M| \gg 1$ and this Gaussian pump pulse profile, evaluating (6) gives a Gaussian impulse response with width $\delta\tau_{\text{out}}$, which, when referred to the input, results in a resolution that is equal to the undispersed pump pulsewidth

$$\delta\tau_{\text{in}} = \delta\tau_{\text{out}}/|M| = \Delta\tau_{p_0}. \quad (8)$$

Expressed in terms of the f -number, $\delta\tau_{\text{in}} = .44T_2 f^\#$ where T_2 is an optical period of the output signal. Systems may also be constructed for compression, and, when $|M| \ll 1$, we find that the limitation on the resolvable feature that can be generated at the output of the system is also equivalent to the undispersed pump profile

$$\delta\tau_{\text{out}} = \delta\tau_{\text{in}}|M| = \Delta\tau_{p_0}. \quad (9)$$

This definition of resolution does not include aberrations that may exist in the temporal imaging system or the finite resolution of the final signal recording system. Although some applications may require a more stringent resolution criterion, it is reasonable to expect a temporal imaging system resolution comparable to the pump pulse’s transform-limited duration.

III. RESOLUTION LIMIT DUE TO GROUP VELOCITY MISMATCH

Constructing a high-fidelity parametric temporal imaging system requires efficient conversion of all input and pump

spectral components to their sum or difference frequencies. While there are well-established methods for matching the phase velocities of signals in anisotropic nonlinear crystals, group velocity mismatch (GVM) causes spectral components near the phase-matched carrier frequencies to shift out of phase with the nonlinear polarization and thereby reduces their conversion efficiency. Minimizing this phase shift by limiting the interaction length produces a broader bandwidth signal but with reduced peak conversion than could be achieved with longer crystals. Designing a system for optimum performance therefore requires understanding the effects spectral filtering produces in the system.

An extensive analysis has been done on phase and group velocity mismatch effects for pulsed second-harmonic generation [27] and sum-frequency generation [28]. The general result including both of these effects is

$$\begin{aligned} A_2(\tau) \propto & \chi_{\text{eff}}^{(2)} L \int_{-\infty}^{+\infty} d\Omega \exp(i\Omega\tau) \\ & \times \int_{-\infty}^{+\infty} d\Omega' \mathcal{A}_p(\Omega - \Omega') \mathcal{A}_1(\Omega') \\ & \times \exp(i(\Delta k + \delta\beta'_{2,p}\Omega + \delta\beta'_{p,1}\Omega')L/2) \\ & \times \text{sinc}((\Delta k + \delta\beta'_{2,p}\Omega + \delta\beta'_{p,1}\Omega')L/2) \end{aligned} \quad (10)$$

where

$$\begin{aligned} \delta\beta'_{2,p} & \equiv \frac{1}{v_g(\omega_2)} - \frac{1}{v_g(\omega_p)}, \\ \delta\beta'_{p,1} & \equiv \frac{1}{v_g(\omega_p)} - \frac{1}{v_g(\omega_1)} \end{aligned} \quad (11)$$

and $\chi_{\text{eff}}^{(2)}$ is the effective nonlinear susceptibility for the chosen material and mixing configuration, L is the interaction length in the crystal, and the same notation for input and output envelopes are used as in Fig. 1(c). The integral with respect to Ω is an inverse Fourier transform whereas the second integral resembles a convolution, except that it contains additional amplitude and phase functions. Although in general a laborious equation to actually use in calculations, it demonstrates the complicated frequency-domain filtering that occurs as a result of GVM. Let’s assume that phase velocities are matched by design, $\Delta k = 0$, and consider two simplifying cases from which we can gain more insight into the meaning of (10).

A. Output Spectral Filtering

If, for example, the group velocities of the input and pump were matched, then $\delta\beta'_{p,1} = 0$. This could occur in the degenerate case where the carrier of the pump is the same as that of the signal, $\omega_p = \omega_1$, and noncollinear, Type-I phase matching is used. In this case, (10) becomes

$$A_2(\tau) \propto \chi_{\text{eff}}^{(2)} L \mathcal{F}^{-1}\{[A_p(\Omega) * A_1(\Omega)]\mathcal{B}(\Omega)\} \quad (12)$$

where

$$\mathcal{B}(\Omega) = \exp(i\delta\beta'_{2,p}L\Omega/2) \text{sinc}(\delta\beta'_{2,p}L\Omega/2) \quad (13)$$

is the resulting spectral filtering function. It limits the bandwidth of the transmitted spectral intensity $|B(\Omega)|^2$ to

$$\delta\Omega_{\text{out}} = 0.89(2\pi)/(\delta\beta'_{2,p}L)_{\text{FWHM}}. \quad (14)$$

We now have an inverse Fourier transform of a spectral filter function times a convolution. Instead of (4), the output of the time lens in this case is

$$A_2(\tau) \propto [A_1(\tau)A_p(\tau)] * B(\tau) \quad (15)$$

where

$$B(\tau) = \frac{1}{\delta\beta'_{2,p}L} \text{rect}\left(\frac{\tau}{\delta\beta'_{2,p}L} + \frac{1}{2}\right) \quad (16)$$

and

$$\text{rect}(x) = \begin{cases} 1, & |x| \leq 1/2 \\ 0, & \text{otherwise.} \end{cases} \quad (17)$$

The ideal output of the time lens is convolved with a rectangular pulse having a width $\Delta\tau_{g2,p} = \delta\beta'_{2,p}L$, which corresponds to the difference in group delays of the upconverted signal and the pump pulse as they propagate a distance L in the crystal. Including this filtering effect in the impulse response derivation presented in [6] gives an effective impulse response for the imaging system equal to the ideal response convolved with (16), $[C(\tau)\tilde{h}(\tau - \tau'_0)] * B(\tau)$. Expressed in terms of the ideal impulse response, the superposition integral (7) becomes

$$A_{\text{out}}(\tau) = C(\tau)[\tilde{h}(\tau) * A_{\text{in}}(\tau/M)] * B(\tau). \quad (18)$$

We see that this filtering acts as a blurring at the output of what would otherwise be an ideal system.

It is important to recognize that, while the shape of the spectral filtering profile $B(\Omega)$ in (13) results from a GVM in the crystal, its effective location after the lens produces the same result as any other filtering that may occur at the output of the imaging system. For example, the transmission of the output dispersive network $\mathcal{T}_2(\Omega)$ can also be considered by convolving the right side of (18) with $\mathcal{F}^{-1}\{\mathcal{T}_2(\Omega)\}$, or simply by treating $B(\Omega)\mathcal{T}_2(\Omega)$ as one combined filter function. For the rest of this paper, we will assume $\mathcal{T}_2(\Omega)$ is constant over the bandwidth of interest and can therefore be ignored.

The GVM filtering effect would not significantly change the resolution of the system if

$$\Delta\tau_{g2,p} \ll \delta\tau_{\text{out}} \quad (19)$$

but it can have other effects as well. The interaction of the filter $B(\Omega)$ with the residual chirp across the image due to $C(\tau)$ produces a source of attenuation in the output as a function of image time, in other words, a roll-off in the field of view (FOV). The FOV will be discussed further in Section IV, but what is important here is that attempting to balance having a wide FOV and strong conversion efficiency necessitates $\Delta\tau_{g2,p}$ be on the order of $\Delta\tau_{p0}$. If the system is designed for large magnification, then $\delta\tau_{\text{out}} \approx |M|\Delta\tau_{p0}$ and $\Delta\tau_{g2,p}$ will be much smaller than the normal system response. The width of the actual response is nearly unaffected. If the system is designed for small magnification or compression, then the amount of blurring this would

cause is comparable to the ideal resolution $\delta\tau_{\text{out}} \approx \Delta\tau_{p0}$, and it should be carefully considered.

B. Input Spectral Filtering

Another interesting case is when the group velocity of the pump and output signals are matched. In this case, $\delta\beta'_{2,p} = 0$ and the output of the crystal (10) simplifies to

$$A_2(\tau) \propto \chi_{\text{eff}}^{(2)} \mathcal{L}\mathcal{F}^{-1}\{A_p(\Omega) * [A_1(\Omega)\tilde{B}(\Omega)]\} \quad (20)$$

where

$$\tilde{B}(\Omega) = \exp(i\delta\beta'_{p,1}L\Omega/2) \text{sinc}(\delta\beta'_{p,1}L\Omega/2). \quad (21)$$

The spectral filtering now acts directly on the input signal, in effect limiting the bandwidth of the input to

$$\delta\Omega_{\text{in}} = 0.89(2\pi)/(\delta\beta'_{p,1}L)_{\text{FWHM}}. \quad (22)$$

Evaluating the inverse Fourier transform using the convolution theorem gives the time lens output

$$A_2(\tau) \propto [A_1(\tau) * \tilde{B}(\tau)] A_p(\tau) \quad (23)$$

where

$$\tilde{B}(\tau) = \frac{1}{\delta\beta'_{p,1}L} \text{rect}\left(\frac{\tau}{\delta\beta'_{p,1}L} + \frac{1}{2}\right). \quad (24)$$

Evaluating the actual system impulse response in this case results in the ideal response $\tilde{h}(\tau - \tau'_0)$ convolved with a magnified group delay difference function $\tilde{B}(\tau/M)$. The output of the system is a convolution of the ideal image and these functions

$$A_{\text{out}}(\tau) = C(\tau)[\tilde{h}(\tau) * A_{\text{in}}(\tau/M) * \tilde{B}(\tau/M)]. \quad (25)$$

The filter $\tilde{B}(\Omega)$ was the result of GVM but its effect is the same as a filter at the input to the system. Another spectral filter source such as the transmission of the input dispersive system $\mathcal{T}_1(\Omega)$ can also be considered by treating $\tilde{B}(\Omega)\mathcal{T}_1(\Omega)$ as one combined filter function or by including the inverse transformed and magnified function $\tilde{T}_1(\tau/M)$ in the convolution of (25). For now, we will assume $\mathcal{T}_1(\Omega)$ is constant over the bandwidth of interest.

We can ignore the blurring that results from GVM between the pump and the input signals if their group delay difference in the crystal $\Delta\tau_{gp,1} = \delta\beta'_{p,1}L$, magnified by the system, is much smaller than the ideal impulse response

$$|M|\Delta\tau_{gp,1} \ll \delta\tau_{\text{out}}. \quad (26)$$

This condition is difficult to meet for a system with large magnification since the impulse response is approximately the width of a magnified undispersed pump pulse $\delta\tau_{\text{out}} \approx |M|\Delta\tau_{p0}$. To do so would generally require a reduction of the interaction length L , producing a corresponding reduction in nonlinear conversion efficiency. If instead we considered a system with strong compression $|M| \ll 1$, the impulse response width is approximately that of the undispersed pump pulse $\delta\tau_{\text{out}} \approx \Delta\tau_{p0}$ but, because of the compression, (26) can still be easily satisfied and the blurring effect can be ignored.

IV. FIELD OF VIEW AND NUMBER OF RESOLVABLE POINTS

There are a number of interesting differences between spatial and temporal imaging systems that make the concept of field of view uniquely different in a temporal system. First of all, spatial imaging is a three-dimensional problem. We may describe the spreading of the envelope function in (x, y) , orthogonal to the direction of propagation z . Temporal imaging involves two coupled, collinear traveling-wave coordinates τ and ξ and produces a spreading of the waveform in the same direction as it is propagating. We may aid the understanding of the temporal imaging process by drawing temporal ray diagrams [8], [29] having orthogonal axes. With the local time τ on the vertical axis and the GDD $\phi'' = \xi\beta''$ on the horizontal axis, each ray represents a space-time path for a spectral component $\Omega = \omega - \omega_0$ in a traveling-wave coordinate system moving at the group velocity of the carrier frequency ω_0 . However, care must be taken not to assign meaning in the time domain to multidimensional geometric projection effects such as vignetting that occur in space. For example, in a spatial system, a cone of rays centered around a high spatial frequency (large angle) will see an effectively smaller lens due to the geometric projection of the lens in the direction of the rays. This effect is one limitation to the FOV in spatial systems. In time-domain systems, the effective aperture time is unchanged for higher frequency spectral components. The impression that it does change is an artifact of the two-dimensional representation. Spectral filtering effects can cause a similar roll-off in the transmitted signal but the mechanism is independent of the aperture time and not directly analogous to the processes that occur in spatial systems.

The concept of a stop or pupil in spatial imaging is analogous to a fast temporal shutter in temporal imaging and requires an active high-speed modulation that is not easily obtained. Besides the pupil of the time lens itself $P(\tau)$, the other common temporal aperture is a field stop that results from a limited record length of the final signal recording system. Although this must be considered, we will assume here that it is long enough not to be a fundamental limitation to the combined system.

More common than stops in temporal imaging are elements that have a finite transmission bandwidth, with the dominant limitation due to group delay mismatch in the crystal. Equation (14) or (22) defines a finite spectral FOV $\delta\Omega$, analogous to a limited angular FOV in spatial systems, as depicted in Fig. 2. Consider what happens if an impulse is scanned through the input, i.e., $A_{\text{in}}(\tau) = \delta(\tau - \tau_0)$. After propagating through the input dispersion, the infinite bandwidth of the impulse would spread the pulse infinitely in time with the spectral components centered at $\Omega = -\tau_0/\phi_1''$ overlapping with the center of the time lens aperture $P(\tau)$ at $\tau = 0$. If there was no filtering effect, then, for any input time τ_0 , the output would just shift to a different spectral region. The bandwidth and amount of energy out of the system would remain constant, producing an infinite temporal field of view. In reality, we know that the transmission bandwidth, or spectral FOV, will be limited to some maximum $\delta\Omega$. This produces a roll-off in the temporal FOV

$$\text{FOV}_{\text{max}} = |\phi_1''| \delta\Omega. \quad (27)$$

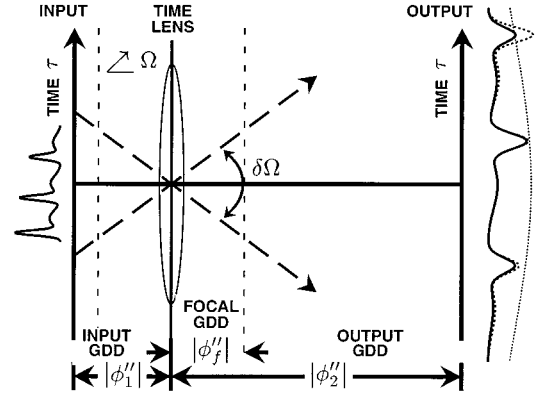


Fig. 2. Spectral filtering produces a finite spectral FOV $\delta\Omega$ analogous to an angular FOV in spatial systems.

This FOV represents the maximum extent expected because it assumes an infinite input bandwidth and is therefore analogous to the range over which a point source can be viewed in a spatial system. Since the input field in spatial imaging systems is often made up of diffusely scattering surfaces, the input features have a tremendous spatial frequency content, and this approach typically produces an accurate representation. In contrast, if the signal was a beam of light with limited spatial frequency content, there would be a much narrower range of positions over which an image of the input beam profile could be viewed. In temporal imaging, ultrashort features (pulses) are nearly transform limited and thus much more analogous to imaging beams.

In reality, the input signal has a limited bandwidth and short temporal features have a finite extent after propagating through the input dispersion. Depending on their initial time and central frequency, they may or may not overlap well with the time lens or may be attenuated due to filtering effects. Let's assume that the input signal we wish to study is made up of short features $A_0(\tau)$. The FOV would then be the width of the energy out of the system $U(\tau_0)$ as a function of the input time τ_0 of this feature [i.e., the width of $U(\tau_0) \propto \int |A_{\text{out}}(\tau; \tau_0)|^2 d\tau$ for $A_{\text{in}}(\tau) = A_0(\tau - \tau_0)$]. An exact solution including the finite nature of the input temporal features, the GVM effects described in (10), the finite duration of the time lens, and any other spectral filtering sources requires numerical evaluation.

A simplifying situation arises when the input and pump bandwidths are much narrower than any spectral filtering effects, $\Delta\omega_0, \Delta\omega_p \ll \delta\Omega$, and the central frequency of the feature is the same as the carrier frequency for the total envelope, $\Omega = 0$. We may then ignore the filtering effects and consider only the finite duration (or bandwidth) of the pump and input signals. The output energy as a function of the input time results in a cross correlation of the time lens pump profile and the dispersed input feature

$$U(\tau_0) \propto \int_{-\infty}^{+\infty} |A_1(\tau - \tau_0)A_p(\tau)|^2 d\tau \quad (28)$$

where $A_1(\tau - \tau_0) = G_1(\tau) * A_0(\tau - \tau_0)$ is the dispersed profile of an input feature $A_0(\tau - \tau_0)$ and $G_1(\tau) = (1/\sqrt{2\pi i\phi_1''}) \exp(i\tau^2/2\phi_1'')$ is the ideal response of the

input GDD. Assuming both envelope profiles are Gaussian results in the FOV

$$\text{FOV} = \sqrt{\Delta\tau_p^2 + \Delta\tau_1^2} \quad (29)$$

where the initial input feature we wish to record is assumed so highly dispersed that its bandwidth $\Delta\omega_0$ produces a pulsewidth $\Delta\tau_1 \approx |\phi_1''| \Delta\omega_0$ at the time lens. For systems with large magnification, the magnitude of the input and focal dispersions are approximately equal $|\phi_1''| \approx |\phi_f''|$ and the FOV can be expressed in terms of the bandwidths and focal GDD

$$\text{FOV} \approx |\phi_f''| \sqrt{\Delta\omega_p^2 + \Delta\omega_0^2} \quad (30)$$

$$\approx |\phi_f''| \Delta\omega_p \sqrt{1 + \left(\frac{\Delta\omega_0}{\Delta\omega_p}\right)^2}. \quad (31)$$

If the bandwidth of the feature being studied is small, $\Delta\omega_0 \ll \Delta\omega_p$, then the FOV is simply the duration of the pump pulse, $\text{FOV} \approx |\phi_f''| \Delta\omega_p \approx \Delta\tau_p$. On the other hand, if its bandwidth is much larger than that of the pump pulse, $\Delta\omega_0 \gg \Delta\omega_p$, the FOV will be determined by the duration of the dispersed input feature, $\text{FOV} \approx |\phi_f''| \Delta\omega_0 \approx \Delta\tau_1$.

The number of resolvable points is given by the FOV divided by the resolution at the input, $N = \text{FOV}/\delta\tau_{\text{in}}$. When the system is constructed for large magnification, this results in

$$N \approx \frac{\Delta\tau_p}{\Delta\tau_{p0}} \sqrt{1 + \left(\frac{\Delta\omega_0}{\Delta\omega_p}\right)^2} \quad (32)$$

which is simply the amount the pump pulse was stretched from its initial transform-limited width times an input bandwidth enhancement factor. The broader the input bandwidth, the larger the number of resolvable points, but, if the system was designed to fully resolve the fine detail of the input signal, these two bandwidths will be comparable $\Delta\omega_p \approx \Delta\omega_0$ and the number of resolvable features is determined primarily by the pump pulse stretch factor $N \approx \sqrt{2}(\Delta\tau_p/\Delta\tau_{p0})$.

When a system is designed for strong compression, $|M| \ll 1$, the input dispersion is much larger than the focal dispersion, $|\phi_1''| = |\phi_2''/M| \approx |\phi_f''/M|$. In this case, the FOV (29) can be expressed as

$$\text{FOV} \approx |\phi_f''| \Delta\omega_p \sqrt{1 + \left(\frac{\Delta\omega_0}{M\Delta\omega_p}\right)^2}. \quad (33)$$

Since the input resolution in the case of strong compression is $\delta\tau_{\text{in}} \approx \Delta\tau_{p0}/|M|$, the number of resolvable features is given by

$$N \approx \frac{|M|\Delta\tau_p}{\Delta\tau_{p0}} \sqrt{1 + \left(\frac{\Delta\omega_0}{M\Delta\omega_p}\right)^2} \quad (34)$$

$$\approx \frac{\Delta\tau_p}{\Delta\tau_{p0}} \sqrt{M^2 + \left(\frac{\Delta\omega_0}{\Delta\omega_p}\right)^2}. \quad (35)$$

A reasonable expectation for a system performing compression is that the input waveform varies slowly in comparison to the system resolution. The bandwidth of each resolvable feature at the input is small, increased to near that of the pump

at the output of the system. Thus, a system designed for maximum compression will have $\Delta\omega_0/\Delta\omega_p \approx |M|$, resulting in $N \approx \sqrt{2}|M|(\Delta\tau_p/\Delta\tau_{p0})$ resolvable input features.

V. CONCLUSIONS

With standard birefringent phase-matching techniques, GVM in the nonlinear crystal produces filtering effects in the system. The bandwidth of the filter decreases as the interaction length is increased to get maximum conversion efficiency, thus there is a tradeoff between the strength of the parametric image signal and the temporal performance of the system.

The blurring effect of GVM is magnified in a temporal imaging system. This works both to our advantage and disadvantage. In systems with large magnification, the GVM between the input and pump signals must be kept small, but blurring due to a GVM between the pump and output signal is less significant to the system resolution because the bandwidth of each resolvable feature has been reduced by the temporal imaging process. Likewise, in systems configured for compression, the GVM between the output and pump must be kept small because the bandwidth of each resolvable feature is the largest at the output, but the GVM between the input and pump is much less significant to the resolution.

Information from different temporal regions of the input waveform are transmitted through the system at slightly different frequencies. In fact, the frequency chirp imparted by the time lens, scaled by the magnification, remains in the final temporal image. Spectral filtering effects will therefore also produce additional roll-off in the temporal FOV.

It may be possible to mitigate the problems resulting from GVM in the nonlinear crystal by using quasi-phase matching [30]. This technique allows phase matching at orientations in crystals not otherwise possible with standard phase matching and can produce a high effective nonlinear susceptibility $\chi_{\text{eff}}^{(2)}$. Varying the poling period allows different spectral components to be properly phase matched at different locations in the crystal producing efficient broadband conversion. The interplay between the group velocities of the signals and the location at which each spectral component is generated also produces an engineerable effective group delay dispersion [31], [32]. This effective GDD could be combined with (or possibly replace) other dispersive delay lines in the temporal imaging system.

REFERENCES

- [1] P. Tournois, J.-L. Verner, and G. Biennu, "Sur l'analogie optique de certains montages électroniques: Formation d'images temporelles de signaux électriques," *C. R. Acad. Sci.*, vol. 267, pp. 375–378, 1968.
- [2] W. J. Caputi, "Stretch: A time transformation technique," *IEEE Trans. Aerosp. Electron. Syst.*, vol. AES-7, pp. 269–278, 1971.
- [3] L. S. Telegin and A. S. Chirkin, "Reversal and reconstruction of the profile of ultrashort light pulses," *Sov. J. Quantum Electron.*, vol. 15, pp. 101–102, 1985.
- [4] S. A. Akhmanov, V. A. Vysloukh, and A. S. Chirkin, "Self-action of wave packets in a nonlinear medium and femtosecond laser pulse generation," *Sov. Phys. Usp.*, vol. 29, pp. 642–677, 1987.
- [5] B. H. Kolner and M. Nazarathy, "Temporal imaging with a time lens," *Opt. Lett.*, vol. 14, pp. 630–632, 1989, erratum vol. 15, p. 655, 1990.
- [6] B. H. Kolner, "Space-time duality and the theory of temporal imaging," *IEEE J. Quantum Electron.*, vol. 30, pp. 1951–1963, Aug. 1994.
- [7] P. Naulleau and E. Leith, "Stretch, time lenses, and incoherent time imaging," *Appl. Opt.*, vol. 34, no. 20, pp. 4119–4128, 1995.

- [8] C. V. Bennett and B. H. Kolner, "Principles of parametric temporal imaging—Part I: System configurations," *IEEE J. Quantum Electron.*, vol. 36, pp. 430–437, Apr. 2000.
- [9] P. Tournois, "Analogie optique de la compression d'impulsion," *C. R. Acad. Sci.*, vol. 258, pp. 3839–3842, Apr. 1964.
- [10] A. Papoulis, *Systems and Transforms with Applications in Optics*. New York, NY: McGraw-Hill, 1968.
- [11] S. A. Akhmanov, A. S. Chirkin, K. N. Drabovich, A. I. Kovrigin, R. V. Khokhlov, and A. P. Sukhorukov, "Nonstationary nonlinear optical effects and ultrashort light pulse formation," *IEEE J. Quantum Electron.*, vol. QE-4, pp. 598–605, 1968.
- [12] S. A. Akhmanov, A. P. Sukhorukov, and A. S. Chirkin, "Nonstationary phenomena and space-time analogy in nonlinear optics," *Sov. Phys.—JETP*, vol. 28, pp. 748–757, 1969.
- [13] E. B. Treacy, "Optical pulse compression with diffraction gratings," *IEEE J. Quantum Electron.*, vol. QE-5, pp. 454–458, 1969.
- [14] J. W. Goodman, *Introduction to Fourier Optics*. New York, NY: McGraw-Hill, 1968.
- [15] B. H. Kolner, "Generalization of the concepts of focal length and f -number to space and time," *J. Opt. Soc. Amer. A*, vol. 11, no. 12, pp. 3229–3234, Dec. 1994.
- [16] J. A. Giordmaine, M. A. Duguay, and J. W. Hansen, "Compression of optical pulses," *IEEE J. Quantum Electron.*, vol. QE-4, pp. 252–255, 1968.
- [17] D. R. Grischowsky, "Optical pulse compression," *Appl. Phys. Lett.*, vol. 26, pp. 566–568, 1974.
- [18] J. E. Bjorkholm, E. H. Turner, and D. B. Pearson, "Conversion of cw light into a train of subnanosecond pulses using frequency modulation and the dispersion of a near-resonant atomic vapor," *Appl. Phys. Lett.*, vol. 26, pp. 564–566, 1975.
- [19] J. K. Wigmore and D. R. Grischowsky, "Temporal compression of light," *IEEE J. Quantum Electron.*, vol. QE-14, pp. 310–315, 1978.
- [20] B. H. Kolner, "Active pulse compression using an integrated electro-optic phase modulator," *Appl. Phys. Lett.*, vol. 52, no. 14, pp. 1122–1124, 1988.
- [21] A. A. Godil, B. A. Auld, and D. M. Bloom, "Picosecond time-lenses," *IEEE J. Quantum Electron.*, vol. 30, pp. 827–837, Mar. 1994.
- [22] B. H. Kolner, C. V. Bennett, and R. P. Scott, "Space-time duality and temporal imaging," *Proc. SPIE OE/LASE*, vol. 2116, 1994. Paper 37.
- [23] M. T. Kauffman, A. A. Godil, W. C. Banyai, and D. M. Bloom, "Applications of time lens optical systems," *Electron. Lett.*, vol. 29, pp. 268–269, 1993.
- [24] C. V. Bennett, R. P. Scott, and B. H. Kolner, "Temporal magnification and reversal of 100 Gb/s optical data with an up-conversion time microscope," *Appl. Phys. Lett.*, vol. 65, no. 20, pp. 2513–2515, Nov. 1994.
- [25] C. V. Bennett and B. H. Kolner, "Upconversion time microscope demonstrating $103\times$ magnification of femtosecond waveforms," *Opt. Lett.*, vol. 24, no. 11, pp. 783–785, June 1999.
- [26] —, "Parametric temporal imaging," in *Ultrafast Electronics and Optoelectronics, Trends in Optics and Photonics Series*, J. Bowers and W. Knox, Eds: OSA, Aug. 1999, vol. 28, pp. 53–62.
- [27] A. M. Weiner, "Effect of group velocity mismatch on the measurement of ultrashort optical pulses via second harmonic generation," *IEEE J. Quantum Electron.*, vol. QE-19, pp. 1276–1283, Aug 1983. erratum vol. QE-20, p. 449, April 1984.
- [28] A. P. Baronavski, H. D. Ladouceur, and J. K. Shaw, "Analysis of cross correlation, phase velocity mismatch, and group velocity mismatches in sum-frequency generation," *IEEE J. Quantum Electron.*, vol. 29, pp. 580–589, Sept. 1993.
- [29] S. P. Dijaili, A. Dienes, and J. S. Smith, "ABCD matrices for dispersive pulse propagation," *IEEE J. Quantum Electron.*, vol. 26, pp. 1158–1164, June 1990.
- [30] M. M. Fejer, G. A. Magel, D. H. Jundt, and R. L. Byer, "Quasiphase-matched second harmonic generation: Tuning and tolerances," *IEEE J. Quant. Electron.*, vol. 28, pp. 2631–2654, 1992.
- [31] M. A. Arbore, O. Marco, and M. M. Fejer, "Pulse compression during second-harmonic generation in aperiodic quasiphase-matching gratings," *Opt. Lett.*, vol. 22, pp. 865–867, 1997.
- [32] M. A. Arbore, A. Galvanauskas, D. Harter, M. H. Chou, and M. M. Fejer, "Engineerable compression of ultrashort pulses by use of second-harmonic generation in chirped-period-poled lithium niobate," *Opt. Lett.*, vol. 22, pp. 1341–1343, 1997.

Corey V. Bennett (S'95), for a photograph and biography, see p. 437 of the April 2000 issue of this JOURNAL.

Brian H. Kolner (S'79–M'79), for a photograph and biography, see p. 437 of the April 2000 issue of this JOURNAL.